

**DEVELOPMENT OF AN X RAY  
DIFFRACTOMETER AND ITS  
SAFETY FEATURES**

By

Jordan A. Cady

A thesis submitted in partial fulfillment of the  
requirements for the degree of

Bachelor of Science

Houghton College

January 2017

Signature of Author.....

Department of Physics  
January 4, 2017

.....

Dr. Brandon Hoffman  
Associate Professor of Physics  
Research Supervisor

.....

Dr. Mark Yuly  
Professor of Physics

**DEVELOPMENT OF AN X  
RAY DIFFRACTOMETER AND  
ITS SAFETY FEATURES**

By

Jordan A. Cady

Submitted to the Department of Physics  
on January 4, 2017 in partial fulfillment of the  
requirement for the degree of  
Bachelor of Science

**Abstract**

A Bragg-Brentano  $\theta$ - $2\theta$  x ray diffractometer is being constructed at Houghton College to map the microstructure of textured, polycrystalline silver films. A Phillips-Norelco x ray source will be used in conjunction with a 40 kV power supply. The motors for the motion of the  $\theta$  and  $2\theta$  arms, as well as a Vernier Student Radiation Monitor, will all be controlled by a program written in LabVIEW. The entire mechanical system and x ray source are contained in a steel enclosure to ensure the safety of the users.

Thesis Supervisor: Dr. Brandon Hoffman  
Title: Associate Professor of Physics

## TABLE OF CONTENTS

<b>Chapter 1 Introduction.....</b>	<b>6</b>
<b>1.1 History of Interference.....</b>	<b>6</b>
<b>1.2 Discovery of X rays .....</b>	<b>7</b>
<b>1.3 Discovery of Diffraction.....</b>	<b>8</b>
1.3.1 Contributions from Max Von Laue .....	8
1.3.2 Contribution from W.H. Bragg and W.L. Bragg .....	9
<b>1.4 Thin Films and Diffraction.....</b>	<b>10</b>
1.4.1 Diffraction in Metals .....	11
1.4.2 Diffraction in Thin Films .....	11
1.4.3 Advances in X ray Diffraction and Optics.....	12
1.4.4 Effects of Deposition and Annealing on Thin Films .....	12
1.4.5 Texture Transitions in Silver (Ag) Thin Films.....	14
<b>1.5 Thin Film Research at Houghton.....</b>	<b>14</b>
1.5.1 Deposition Chamber.....	15
1.5.2 Atomic Force Microscope.....	15
1.5.3 Phase-Stepping Laser Interferometer.....	15
1.5.4 X ray Diffractometer .....	16
<b>Chapter 2 Theory .....</b>	<b>17</b>
<b>2.1 X ray Sources .....</b>	<b>17</b>
2.1.1 Characteristic X rays.....	17
2.1.2 Bremsstrahlung X rays.....	17
<b>2.2 Interference .....</b>	<b>18</b>
<b>2.3 Crystallography .....</b>	<b>20</b>
2.3.1 Crystal Structure and Orientation .....	<b>Error! Bookmark not defined.</b> 20
<b>2.4 Bragg's Law.....</b>	<b>21</b>
<b>Chapter 3 Apparatus .....</b>	<b>23</b>
<b>3.1 Houghton College X ray Diffractometer .....</b>	<b>23</b>
<b>3.2 X ray Source.....</b>	<b>23</b>
3.2.1 Current X ray Source.....	23
3.2.2 Collimation of X rays .....	24
<b>3.3 Mechanical Design .....</b>	<b>25</b>
3.3.1 The Table.....	25

3.3.2	Arms and Stepper Motors .....	26
3.3.3	Sample Mount .....	26
<b>3.4</b>	<b>Safety Features .....</b>	<b>26</b>
3.4.1	HV Acrylic Box .....	26
3.4.2	Steel Encasement with Interlocks.....	26
<b>Chapter 4</b>	<b>Results .....</b>	<b>29</b>
	<b>Intensity of X ray Source.....</b>	<b>29</b>
<b>Chapter 5</b>	<b>Conclusion.....</b>	<b>32</b>
<b>5.1</b>	<b>Current Status.....</b>	<b>32</b>
5.1.1	X ray Source.....	32
5.1.2	Steel Encasement .....	32
5.1.3	LabVIEW Program .....	32
5.1.4	Stepper Motors.....	33
<b>5.2</b>	<b>Future Plans .....</b>	<b>33</b>
5.2.1	Interlocking System .....	33
5.2.2	Cooling System with Flowmeter.....	33
5.2.3	Web Camera.....	34

## TABLE OF FIGURES

Figure 1. Picture of Newton's Rings.....	6
Figure 2. Crookes tube schematic.....	7
Figure 3. Photograph of Rontgen's wife's hand.....	7
Figure 4. Photograph of a compass.....	7
Figure 5. Diffraction pattern of nickel sulphate.....	8
Figure 6. Planar reflection of x rays.....	9
Figure 7. Two-dimensional crystal lattice.....	9
Figure 8. Bragg's x ray spectrometer.....	10
Figure 9. (100) and (111) crystal orientations .....	13
Figure 10. Houghton deposition chamber.....	16
Figure 11. Houghton atomic force microscope.....	16
Figure 12. Houghton phase-stepping interferometer.....	16
Figure 13. Houghton x ray diffractometer.....	16
Figure 14. Characteristic x ray production.....	18
Figure 15. Bremsstrahlung x ray production.....	18
Figure 16. Various crystal unit cells.....	21
Figure 17. Three-dimensional stacking.....	21
Figure 18. Bragg's law diagram.....	22
Figure 19. X ray source circuit diagram.....	24
Figure 20. Collimator.....	25
Figure 21. Bragg-Brentano x ray diffractometer.....	25
Figure 22. Stepper motor.....	28
Figure 23. Thin film sample mount.....	28
Figure 24. High-voltage acrylic box.....	28
Figure 25. Steel encasement.....	28
Figure 26. Graph of intensity of the x ray source vs. emission current.....	29

## Chapter 1

### INTRODUCTION

#### 1.1 History of Interference

In the early 1700s, Sir Isaac Newton discovered the historical “Newton’s Rings.” In his experiment a plano-convex lens was placed on a sheet of glass convex side down. He allowed light to fall normally on the lens. When viewing the reflected rays concentric circles had formed, having a bright center with the rings growing dimmer depending on their distance from the center. This phenomenon is due to destructive interference of light waves [1]. A diagram of Newton’s rings can be seen in Figure 1.

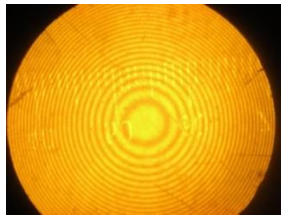


Figure 1: Picture displaying Newton’s rings caused by the destructive interference of light waves. Figure taken from Ref. [2].

In 1802, Thomas Young expanded on many of Newton’s theories and published his lecture “On the Theory of Light and Colours” describing different interference phenomena including constructive and destructive interference [3]. In 1803, Young completed his famous double slit experiment. Young allowed a beam of homogeneous light to fall on a screen with two very small holes or slits. These holes can be considered centers of divergence from which light is diffracted in every direction. The results of the two newly formed beams were seen on a surface placed on the far side of the holes. On the surface, the light was divided by dark stripes due to the destructive interference between the two newly formed beams [4]. The results of this experiment not only gave a further understanding of interference, but ultimately showed light’s wave-particle duality. Interference is explained in further detail in Section 2.2.

## 1.2 Discovery of X rays

On November 8<sup>th</sup>, 1895 a new type of electromagnetic radiation was discovered by Wilhelm Conrad Rontgen, which he called x rays [5]. At the time he was experimenting with electrical current flow through gases at low pressure. For these experiments he used what is called a Crookes tube. The tube contained a gas at low pressure and had a high voltage applied to it via a large inductor coil. Once the high voltage was applied to the tube, electrons were emitted from the cathode and accelerated out into the open area of the tube. They would either hit the target that was placed in the center of the tube or continue past it and collide with the front wall causing a dim glow to appear around a shadow of the target.

For the particular experiment where Rontgen made his discovery, he placed black paper around the outside of the tube and ran the experiment in a room without any visible light. He found that, when he placed a florescent screen of barium-platinum-cyanide within two meters of the tube, it began to glow due to the emitted x rays [5]. He began to experiment with these new rays, taking images of various objects and elements, of which included his wife's hand and a compass enclosed in a metal case.

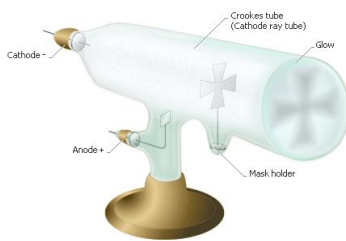


Figure 2: Diagram of a Crookes tube. Electrons are emitted from the cathode and are pulled into the tube, towards the target, by the anode. The electrons that do not collide with the target hit the end of the tube, creating a florescent light. Figure taken from Ref [6].



Figure 3: Photograph of Rontgen's wife's hand. Her ring appears darker in the image since it has a density that is greater than that of bone. Figure taken from Ref [7].

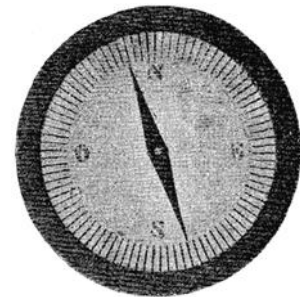


Figure 4: Photograph of a compass card and needle enclosed in a metal case. Figure taken from Ref. [7].

## 1.3 Discovery of Diffraction

### 1.3.1 Contributions from Max Von Laue

In 1914, Max Von Laue received the Nobel Prize for Physics for his discovery of the diffraction of x rays on crystals. In his Nobel lecture titled “Concerning the detection of x ray interferences”, he discussed his idea of the ability for x rays to penetrate a crystalline lattice structure [8]. This is possible because the spacing between the atomic layers of a crystal is on the same order of magnitude as the wavelength of the x rays. If the wavelength of the x rays was larger than the spacing between the atomic layers of the crystal, then they would simply reflect off the surface [9]. Von Laue constructed a mathematical theory of diffraction by using a 3D crystal lattice. He showed that if a beam of x rays was directed towards a crystal, a diffraction pattern would form on a photographic plate, arranged in a regular pattern about the primary beam based on what crystal was used. While analyzing his theory further, accompanied by Messrs, Friedrich, and Knipping in the spring of 1912, he tried to account for the fact that out of a large number of possible diffraction directions only certain directions occurred. Typically, when x rays are directed towards a non-crystalline target that scatters them, a continuous pattern is formed all around the target onto a photographic plate. However, in this case, x ray rays were scattered in certain directions only [9]. This phenomenon can be seen in Figure 5. Laue suggested that the x ray source may be the reason for this, whereas William Henry Bragg and William Lawrence Bragg believed the answer to be in the crystalline structure [8].

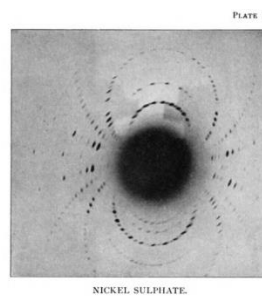


Figure 5: Diffraction pattern of nickel sulphate found by Laue, Messrs, Friedrich, and Knipping. A fine beam of x rays was incident on a nickel sulphate target. Some x rays continued through the target to form the pattern seen on a photographic plate. Figure taken from Ref [9].

### 1.3.2 Contributions from W.H. Bragg and W.L. Bragg

As stated section 1.1.1, W.H. Bragg and W.L. Bragg focused on the crystalline structure to find the driving force behind the results found in Laue's experiments. For simplicity's sake, I will refer to the father and son duo as Bragg. Bragg chose to look at the atoms within a crystal in terms of planes. When a pulse of x rays is incident on a plane of atoms, the pulse is reflected and spreads spherically about the point it reflects. This phenomenon results in a reflected wave front, seen in Figure 6 as P'P' [9]. The wave front is created due to the constructive interference of the x rays. Constructive interference occurs when two or more waves that are in phase, meaning the peaks of the waves are aligned, combine to form one large wave.

This concept can be applied to a two dimensional array of atoms. A crystal in the form of a polygon can be seen in Figure 7. The planes p are all parallel to each other and the upper left face of the crystal. From applying this above phenomenon to the crystal structure, Bragg was able to relate the continuous beam of x rays that is incident on and reflected by the crystal with the spacing of the planes p within the crystal. This relationship is known as Bragg's law. While the basics of this concept are discussed here in this section, the specifics are discussed in Section 2.4.

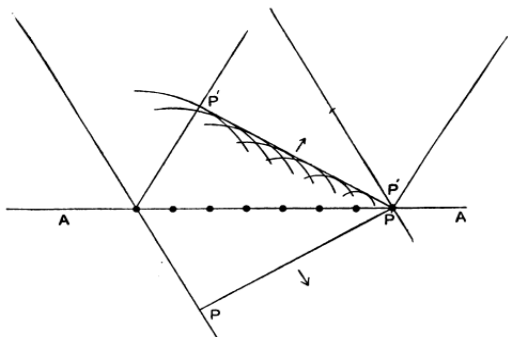


Figure 6: Simple two dimensional example of diffraction. A wave front PP is incident on a plane of atoms, AA. When PP interacts with AA, a reflected wave front P'P' is formed due to the constructive interference of the individually reflected waves. Figure taken from Ref [9].

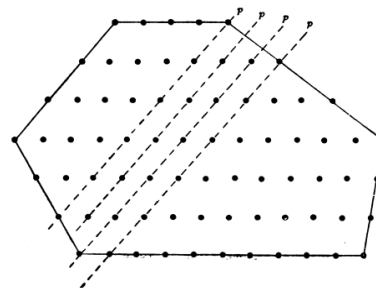


Figure 7: Simple two dimensional crystal. Planes P are parallel to the upper left natural face of the crystal. Figure taken from Ref [9].

For all of his experiments, Bragg used what is known as an x ray spectrometer. A picture of the instrument can be seen in Figure 8. The Bragg x ray spectrometer consisted of an x ray tube that was

encased by a lead-lined wooden box. A small slit was positioned on one of the sides of the box for a beam of x rays to pass through horizontally. A crystal sample was mounted on a revolving table that rotated the crystal through the path of the beam. The x rays that diffracted off of the crystal passed into an ionization chamber that was rotated about the same axis as the crystal table. The ionization chamber was filled with a gas that strongly absorbs x rays, from which a large ionization current was formed. This ionization current then flowed into an electroscope from which they took their data [9]. From viewing the electroscope, the angle of diffraction can be determined. This angle corresponds to the maximum ionization current [9]. Using the angle of diffraction and Bragg's law, the structure of the crystal sample was determined.

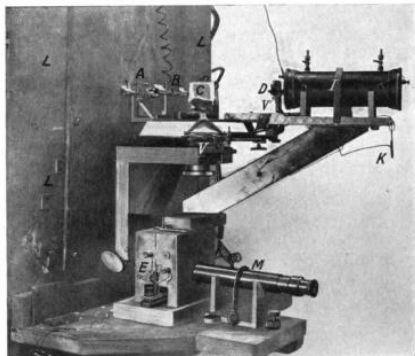


Figure 8: Picture of Bragg's x ray spectrometer. This instrument was used to determine the absolute wavelengths of different types of x rays and the structure of several crystals. The labels are as follows: L-lead, C-crystal, A,B,D- collimation slits, K- earthing key, I- ionization chamber Figure taken from Ref [9].

#### 1.4 Thin Films and X ray Diffraction

X ray diffractometry has been a useful technique in the study of thin metal films. A thin metal film is structured such that its thickness is much smaller than its length and width. The thickness of a thin film can range from nanometers to micrometers. X ray diffraction is important for thin film research in that it allows us to understand how crystals are oriented within a thin film and what percentage of the film is a given orientation. When combining this information with other information about thin films, a greater understanding of their nature can be obtained. It is important to understand the behavior and properties of thin metal films in order to create more advanced, reliable technologies.

#### 1.4.1 *Diffraction in Metals*

With the discovery of powder diffraction in 1916, the use of x rays in the study of metals greatly increased in the 1920s with the completion of World War I. Powder diffraction was a discovery of A. W. Hull, but was almost simultaneously discovered by Debye and Scherrer [10]. With powder diffraction Bragg's geometry is utilized, but the target material is ground into a powder. Since the target material is ground up, the crystals of the substance are oriented in all different directions. This helps in the analysis of polycrystalline materials.

The use of powder diffraction to solve various metallurgical problems during the 1920s led to many advances in the understanding of bulk metals, including iron, copper, and aluminum. Once these metals were manufactured, powder diffraction was used to understand the structure and formation process of the metals and their alloys. In one case, x ray diffraction was used to help in the manufacturing of Nickel-iron alloy powders. These powders were prepared by means of reduction in a mixture of the oxides in certain proportions at high temperatures. The homogeneity of the final powder depends on how efficiently the oxides mixed into the structure of the metals and upon the chosen temperature at which this process took place. X ray diffraction has been used to show insufficient reduction of the oxides into the metals as well as the presence of any unalloyed nickel or iron [11]. From this information, the correct manufacturing conditions were established.

#### 1.4.2 *Diffraction in Thin Films*

As early as the 1930s the differences between electro-deposited thin films and their bulk metal counterparts were being studied. W. A. Wood researched many of these differences including the orientation of the crystals in the thin film compared to the bulk material. He found that while the bulk material had grains oriented at random, the grains in the thin film tended to grow along a given axis in a preferred direction. The orientation of the grains depended greatly on the conditions of the deposition process [12].

With the invention of the transistor, the interest in semiconductors, such as silicon and germanium, grew rapidly. This interest led to more research into how thin film semiconductors behaved. When

impurities are present in a semiconductor, the crystal structure differs from a pure semiconductor. This differing structure leads to addition free or partially free electrons, changing the conductivity of the semiconductor. The process of intentionally introducing impurities into a semiconductor is known as doping.

#### *1.4.3 Advances in X ray Diffraction and Optics*

The invention of both the synchrotron by Edwin M. McMillan and the focusing monochromator by Herbert Friedman in 1945 led to greater efficiency and precision in diffraction research. A synchrotron is a device used to produce high energy charged particles. This type of particle accelerator uses magnetic fields in order to contain the particles to a nearly circular orbit. The particles are accelerated to near the speed of light. The centripetal force acting on the circulating relativistic particles cause them to emit electromagnetic radiation within the vacuum ultraviolet and soft x ray regions tangentially to the circular path of the particles. With the synchrotron, high energy levels of radiation can be attained using either electrons or heavy particles [13]. This high energy radiation can be used in real time x ray diffraction experiments, allowing for any changes in a thin film during the deposition process to be observed [14].

While it is important to have a strong radiation source, it is also important to be able to focus the source radiation and reduce background noise in order to obtain sharp resolution for the diffraction peaks. This is the purpose of the monochromator invented by H. Friedman. A monochromator uses a nearly perfect crystal to permit a certain wavelength of radiation while minimizing any significant background radiation. When paired with a synchrotron source and additional focusing optics, optimal results can be obtained [15].

#### *1.4.4 Effects of Deposition and Annealing on Thin Films*

Due to the differing properties between various metals, films of differing compositions are suitable for different purposes. It is important to research the behaviors of different films in order to understand where they can best be used. At Houghton College the research is focused on Silver thin films, but at Newcastle University a group is focused on Titanium Nitride (TiN) films. Researchers at Newcastle

University are specifically researching the effects of deposition conditions and the annealing process on the resistivity of TiN thin films. Annealing is the process of heating the film over time to liberate intrinsic stress, improve the films structure, as well as surface roughness [16]. The deposition process used by Newcastle is known as reactive sputtering. At Houghton a process known as physical vapor deposition is used. Reactive sputtering is the process where a target, such as titanium, is bombarded by energetic particles in the presence of a gas. The gas reacts with the atoms released from the target to form a coating of a different chemical composition. In this case, the titanium target was surrounded by nitrogen gas. Nitrogen gas was allowed to flow into the chamber containing the titanium target at both 20% and 95% flow rates resulting in different concentrations of nitrogen in the final films. Many processes were used to explore the composition of the TiN films produced, one of which was x ray diffraction. Using Bragg-Brentano geometry, an x ray diffractometer, equipped with a copper x ray source and a 40 kV power supply, was used to determine the volumetric structure of the film. This is the same method we hope to use for the study of silver thin films using the Houghton x ray diffractometer. For the 20% nitrogen flow rate samples, the predominant orientation of the thin film was (111), whereas the predominant orientation for the 95% samples was (100) [17]. A figure of these orientations can be seen in Figure 9. The (100) orientation is simply a cube set on one of its faces. The (111) orientation is that of a cube set on one of its corners.

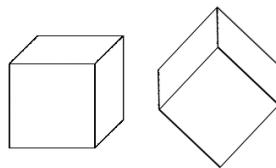


Figure 9: The (100) orientation (left) and the (111) orientation (right) with the normal of the surface towards the top of the page.

It was found that the orientation of the films influenced the resistivity. Films with the (111) orientation had a higher resistivity than that of films with the (100) orientation. Thus, the films with more nitrogen had a lower resistivity since the predominant orientation of high nitrogen content films was found to be (100). After the films were deposited they were annealed, varying time and temperature. It was

shown that resistivity decreased with a longer annealing time and a higher annealing temperature. From these observations it was concluded that the films deposited with a higher concentration of nitrogen are more electrically and thermally stable. This makes them suitable for application such as the gate electrode of MOSFETs, a type of transistor used in microelectronic circuits, or as capacitor electrodes in integrated circuits [16].

#### *1.4.5 Texture Transitions in Silver Thin Films*

A well-known phenomenon of silver thin films is a thickness-dependent texture transformation that occurs during the annealing process. Silver films that are initially in the (111) orientation process will retain this structure after the annealing process if they are sufficiently thin. If the films are sufficiently thick, they transition to a (100) structure [18]. A diagram of these orientations can be seen in Figure 9.

In an effort to understand the driving forces behind this transition, researchers at Cornell University and Houghton College used x ray diffractometry to view the texture evolution of the films as a function of time and temperature during the annealing process. Gradient silver films, with and without a titanium (Ti) adhesive layer were produced in a single run using low-pressure chemical vapor deposition. The gradient was achieved using a linear shutter. For the analysis of the films, a Bragg-Brentano diffractometer was used in conjunction with a copper x ray source to scan the films before and after they were annealed at 400, 500, and 600 °C. In the as-deposited state, the silver films with the Ti interlayers showed a (111) texture fraction near 100%. The silver films without the Ti interlayers showed a (111) texture fraction near 95%. After the annealing process, being consistent with previous observations, thicker films transformed to (100) given enough thermal stimulation, while thinner films stayed (111) [18]. Currently, existing theories do not account for this gradual transition of sufficiently thick (111) films to (100) observed in this experiments. They also fail to explain the kinetics of this gradual transformation and the phenomena that instigate it.

### **1.5 Thin Film Research at Houghton College**

Equipment needed in the study of thin films is being constructed at Houghton College. The equipment consists of a deposition chamber used to produce silver thin films as well as three other

instruments that will be used to examine the films that are produced: an atomic force microscope, phase-stepping laser interferometer, and an x ray diffractometer.

### *1.5.1 Deposition Chamber*

As stated above, the deposition chamber is used to produce silver thin films at this point in time. Within the vacuum chamber that was constructed, 99.99% pure silver pellets are heated such that the silver evaporates and condenses on a silicon substrate forming a thin film. This process takes place in a vacuum to ensure that the resulting thin film is as pure as possible [19].

### *1.5.2 Atomic Force Microscope*

The atomic force microscope is still in its beginning stages. When assembled, it will be used to map the roughness of the surface of a film. To do this, it scans a fine tip, that is on the order of micrometers long and atomically sharp, over the top of a film. The tip is attached to a cantilever that is set to oscillate. The amplitude of oscillation is related to the distance between the tip and sample. To measure this amplitude, a diode laser is aligned such that it reflects off the back of the cantilever onto a quadrant detector. As the cantilever oscillates, the laser spot on the detector oscillates proportionately. The sample is adjusted to hold the distance (and, therefore, amplitude) constant. A topographical map is then constructed from plotting the vertical position of the sample as a function of the horizontal position of the tip. The topographical map of the film's surface will help in modeling the driving forces of the crystal orientation within the film [20].

### *1.5.3 Phase-Stepping Laser Interferometer*

The phase-stepping laser interferometer is near completion. The interferometer produces a topological map of the thin metal film. From the topological map, the curvature of the film can be determined. When the interferometer is completed it will be attached underneath the deposition chamber and used to measure the curvature of the films while they are at elevated temperatures. The determined curvatures will be used to calculate the stresses of the film [21].

### 1.5.4 X ray Diffractometer

The diffractometer is operational, but safety features, such as a steel encasement and a high voltage interlock, need to be completed before tests can be run. The safety features required for the diffractometer are discussed further in Section 3.5. When the safety features are in place, the diffractometer will be used to measure the inter-planar distances of the thin metal films. In turn, this will give the relative volume fractions of the dominant orientations within the thin metal film. The theory behind x ray diffraction will be discussed in the Chapter 2.



Figure 10: Photograph of the Houghton deposition chamber. The frame that will hold the Houghton interferometer is hung below the chamber.

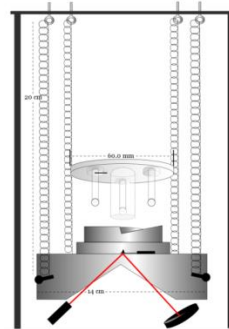


Figure 11: Diagram of the Houghton atomic force microscope with various dimensions included. Figure taken from Ref [22].

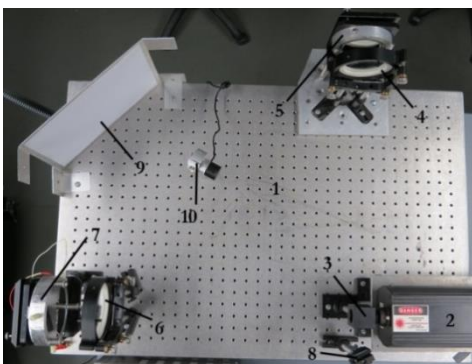


Figure 12: Photograph of the Houghton phase-stepping interferometer. The labeled components are as follows: 1) Optics 2) 632nm Laser 3) Beam Splitter 4) Sample Collimating Lens 5) Sample Mirror 6) Reference Collimating Lens 7) Reference Mirror 8) Image Collimating Lens 9) Screen 10) Webcam. The screen is present for current maintenance purposes. Figure taken from Ref [23].

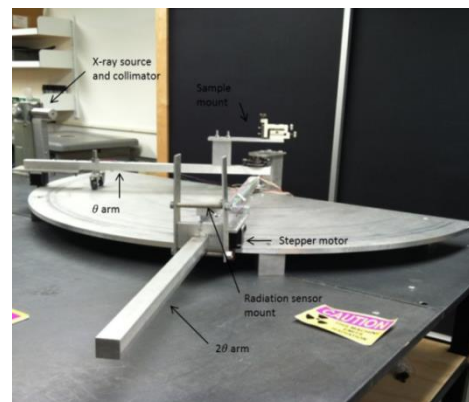


Figure 13: Photograph of the Houghton x ray diffractometer. The apparatus will be discussed in Chapter 3.

## Chapter 2

### THEORY

#### 2.1 X ray Sources

A typical x ray source produces two types of x rays: bremsstrahlung and characteristic x rays. Characteristic x rays are the type of x ray most useful for diffraction since their total energy is known.

##### 2.1.1 Characteristic X rays

To produce characteristic x rays, an incident x ray collides with an electron in the inner shell of an atom resulting in the removal of the inner electron. Both the incident and the inner shell electrons travel away from the atom while an outer shell electron drops down to the hole left by the inner shell electron. When the outer shell electron drops down to the inner shell, it is transitioning from a higher energy state to a lower energy state. The energy released from this transition is seen in the form of a characteristic x ray. The wavelength of the characteristic x ray can be written as

$$\lambda = \frac{hc}{\Delta E}, \quad (1)$$

where  $\Delta E$  is the change in energy from the higher energy level to the lower energy level,  $h$  is Planck's constant, and  $c$  is the speed of light in a vacuum. A diagram of characteristic production can be seen in Figure 14. Since characteristic x rays have discrete energy levels it is easy to calculate the wavelength of the x rays. This type of x ray is useful for diffraction due to the fact that the energy of the x rays that are incident on the target is known [24].

##### 2.1.2 Bremsstrahlung X rays

Bremsstrahlung (Braking) radiation is produced when an electron travels past the nucleus of an atom. The electron's velocity reduces due to the attractive force of the nucleus, thus reducing its kinetic

energy. The energy the electron loses is seen in the form of a bremsstrahlung x ray. The wavelength of the bremsstrahlung x ray can be found using the following equation

$$E_i - E_f = \frac{hc}{\lambda}, \quad (2)$$

where  $E_i$  is the initial energy of the electron and  $E_f$  is the final energy of the electron. A diagram of bremsstrahlung production can be seen in Figure 15. Bremsstrahlung x rays can have a continuous energy spectrum from 0 up to the maximum energy of the electron. It is extremely difficult to know where an x ray is on the spectrum since the electrons would need to be matched up with their corresponding x rays.

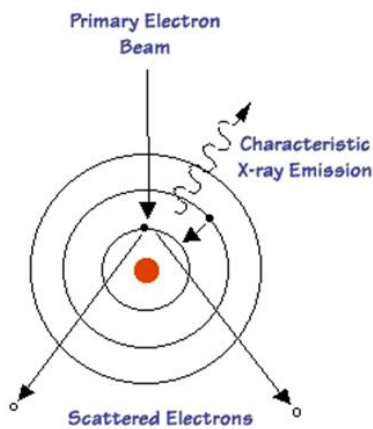


Figure 14: Diagram of characteristic x ray production. Once the inner shell electron is removed, the outer shell electron drops down into the “hole” left by the other electron and an x ray is emitted. Figure taken from Ref. [25].

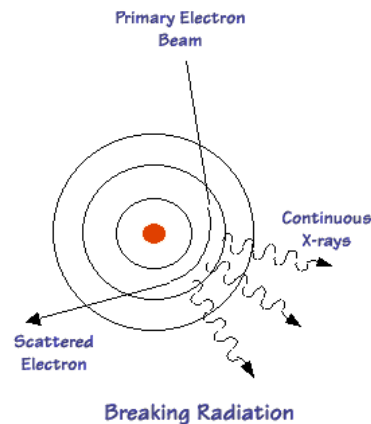


Figure 15: Diagram of bremsstrahlung x ray production. When a high energy electron is attracted by the nucleus and has its path and speed changed, a continuum of x rays is produced. Figure taken from Ref. [25].

## 2.2 Interference

Wave interference is a key part in deriving Bragg’s Law, which is discussed in section 2.4. For Bragg’s law to be true, the characteristic x rays produced by the sources must constructively interfere after they interact with the thin film sample. Interference is essentially a combination of two or more

waves. Constructive interference is when two or more waves combine and form a wave of larger amplitude. Say we have the equations of two different waves of the same frequency and amplitude

$$f(t, \varphi) = A \sin(kx - \omega t) \quad (3)$$

and

$$g(t, \varphi) = A \sin(kx - \omega t + \varphi), \quad (4)$$

where  $A$  is the amplitude,  $k$  is the wave number,  $x$  is the position,  $\omega$  is the angular frequency, and  $\varphi$  is the phase shift. Using the principle of superposition, these waves combine to form a single wave,

$$h(t, \varphi) = A \sin(kx - \omega t) + A \sin(kx - \omega t + \varphi), \quad (5)$$

which can be simplified to

$$h(t, \varphi) = 2A \cos\left(\frac{\varphi}{2}\right) \sin\left(kx - \omega t + \frac{\varphi}{2}\right). \quad (6)$$

Depending on the value of  $\varphi$ , this wave combination will either constructively interfere or destructively interfere. For constructive interference, which is required for Bragg's law to be true, the cosine term must be at a maximum. This occurs when

$$\frac{\varphi}{2} = 0, \pi, 2\pi, \dots \quad (7)$$

or,

$$\varphi = 0, 2\pi, 4\pi, \dots = 2\pi n. \quad (8)$$

For x ray diffraction, the phase difference of the x rays is due to the change in path length caused by the crystal. Since there are  $2\pi$  radians in one full wave,  $\varphi$  can be written as

$$\varphi = \left(\frac{2\pi}{\lambda}\right)P, \quad (9)$$

where  $\lambda$  is the wavelength, and P is the path length difference. Thus, the equation of the interfering waves can be written as

$$h(t, \lambda) = 2A \cos\left(\left(\frac{2\pi}{\lambda}\right)P\right) \sin\left(kx - \omega t + \left(\frac{2\pi}{\lambda}\right)P\right). \quad (10)$$

Since the intensity of the x rays is proportional to the square of  $h(t, \lambda)$ , in time, the sine term averages out to  $1/2$ , resulting in,

$$h(P) = A \cos\left(\left(\frac{2\pi n}{\lambda}\right)P\right). \quad (11)$$

From this it can be seen that  $h(P)$  is a maximum when the path length difference  $P = n\lambda$ .

## 2.3 Crystallography

Understanding the properties and structure of crystals is critical in the derivation of Bragg's Law as well as in the interpretation of results from a diffraction experiment. Bragg's law utilizes the difference in path lengths of x rays reflecting off different parts of a crystal lattice in order to determine the spacing of the planes in the lattice.

### 2.3.1 *Crystal Structure and Orientation*

A single crystal is a solid that consists of a symmetrical three dimensional arrangement of atoms. There are many ways individual crystals can be arranged to form a larger crystal lattice. Seen in Figure 16 are a few possible arrangements of atoms that form a unit cell, the simplest version of a crystal. The most basic form of a unit cell is the simple cubic structure (a), with an atom at each corner of a cube. Silver

atoms are arranged in a face-centered cubic structure (c), with an atom at each corner of a cube as well as at the center of each face on the cube.

The structures seen in Figure 16, as well as all other unit cells, are all formed by 3-dimensional stacking. Layers of atoms are stacked, one on top of the other, to form a crystalline array. An array is a periodic structure made up of many unit cells. Typically, the positioning of the atoms changes from layer to layer. Any structure where the atoms in one layer are stacked directly above the atoms in the layer below is uncommon. An example of this is a simple cubic structure, an array composed of simple cubic unit cells. NaCl, table salt, is a part of this structure category. Another possibility is the cubic close-packed (ccp) structure. Metals, such as gold, silver, and copper, are a part of this structure category. The stacking sequence of the ccp structure can be seen in Figure 17. The structure is stacked in the order A, B, C, and then is repeated to form an array [27].

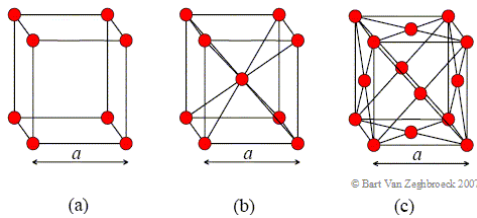


Figure 16: A diagram of various crystal structures. (a) Simple cubic (b) Body-centered cubic (c) Face-centered cubic. Figure taken from Ref. [26].

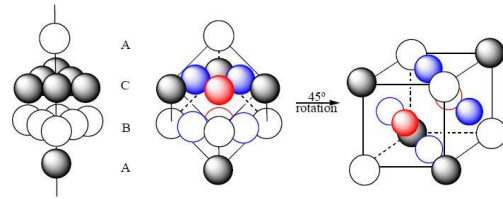


Figure 17: Diagram of the ccp structure, specifically face centered cubic. The figure is stacked A, B, C, then repeated. Rotating the sequence  $45^\circ$  makes the face centered cubic structure evident. Figure taken from Ref [28].

## 2.4 Bragg's Law

Since the wavelengths of x rays are on the same order of magnitude as the spacing of the crystalline planes they can be used to resolve the plane spacing. If a wave front of x rays of wavelength  $\lambda$  reflects off of a crystalline structure at an angle  $\theta$ ,  $\theta$  being the incident angle and the reflected angle, some x rays reflect off of the first plane while others reflect off of the second plane, and so on. If the additional path length traveled by the x rays that went further into the array is an integer multiple of the wavelength, then they constructively interfered. This means that the extra distance traveled by the

x rays is a function of the plane spacing. In Figure 18, there is a basic representation of what is described above, using a simple cubic structure. The x ray that reflects off the lower plane travels an extra distance of  $2d\sin\theta$ . The two reflected x rays constructively interfere when the extra distance traveled is an integer multiple of the wavelength. From this, Bragg's law is written as

$$n\lambda = 2d\sin\theta, \quad (2)$$

where  $n$  is an integer,  $\lambda$  is the wavelength of the x rays,  $d$  is the spacing of the crystalline planes, and  $\theta$  is the angle between the crystal plane and path of the x rays. This shows that the plane spacing in the crystal can be determined with known values of  $\lambda$  and  $\theta$ . Comparing the calculated value of  $d$  with the accepted values of the plane spacings for different orientations, the orientation of the crystals within the thin film can be determined.

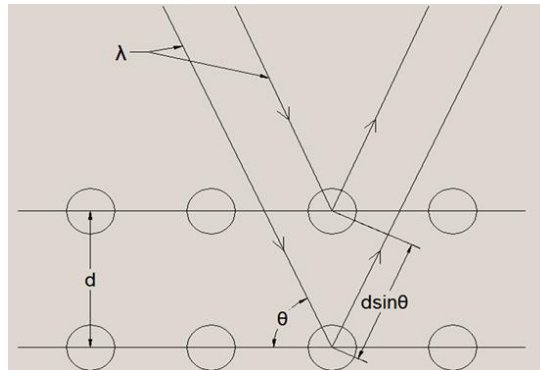


Figure 18: This is a basic visual representation of Bragg's Law.  $\lambda$  is the wavelength of the x rays,  $d$  is the spacing of the crystalline planes, and  $\theta$  is the angle, up from the horizontal, that the x rays strikes the crystal lattice at.

## Chapter 3

### APPARATUS

#### 3.1 Houghton College X ray Diffractometer

In this chapter, details of the construction of the Houghton x ray diffractometer will be discussed. The diffractometer can be split up into four categories: x ray source, mechanical design, electronics, and safety features. All are essential for having a fully functional diffractometer that, for our purposes, can be used for silver thin film research.

#### 3.2 X ray Source

##### 3.2.1 Current X ray Source

The x ray source that is currently in use was salvaged from an x ray generator that the Houghton Physics department had in their possession. The salvaged source was made by Norelco in 1963. The specific x ray tube that is currently being used within the source contains a copper target. The associated  $K\alpha$  and  $K\beta$  wavelengths for copper can be seen in Table 1, along with two other target materials [29].  $K\alpha$  and  $K\beta$  wavelengths for copper are on the same order of magnitude as the plane spacing of crystals. Thus, it can be used to resolve the plane spacing of a crystal.

Table 1:  $K\alpha$  and  $K\beta$  wavelengths for copper, molybdenum, and iron [29].

Target Material	Wavelength of Tube $K\alpha$ (Å)	Wavelength of Tube $K\beta$ (Å)
Copper	1.542	1.392
Molybdenum	0.709	0.632
Iron	1.936	1.756

In order for the tube to produce x rays, an 8 - 12 V battery heats up the low resistance filament inside the tube. The filament then emits electrons, which accelerate towards the copper target. This occurs since the filament is at a negative high voltage and the target is grounded. This current between the filament and the target is known as the emission current. The high voltage power supply being used is a 40 kV supply manufactured by HiTek. Once the electrons interact with the copper target, both bremsstrahlung and characteristic x rays are produced.

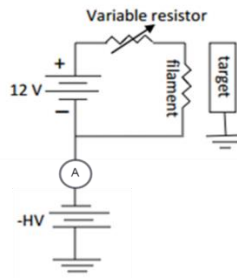


Figure 19: Diagram of the circuit used to generate x rays. High energy electrons that are released from the filament interact with the heavy target material, producing x rays. The target material for the current source is copper.

In order to prevent the target from overheating and breaking, a water cooling system was built into the source. Currently the cooling system consists of two hoses, one feeding the source and the other draining the water from the source. They are simply connected to a sink in the lab.

### 3.2.2 Collimation of X rays

Collimation of the x rays is important for the analysis of the films. Precise knowledge of theta is required for determining the orientations of the crystals in the sample. When x rays are produced within the tube, they travel in all directions. The only x rays that leave the source are through the 6.350 mm window in the side of the casing. A steel cylinder, with a length of 0.1020 m and a diameter of 38.10 mm, is mounted outside of the window. The cylinder has a 6.350 mm hole drilled through the center, this is one of two parts of the collimator. A steel pipe of 3.1750 mm thickness, 0.610 m in length, and 0.01910 m diameter is mounted to the end of the 0.1020 m cylinder and is held in the middle by a temporary mount. A steel pipe was chosen for collimation over a double slit collimator simply for safety purposes. A steel pipe reduces the intensity of the x rays that travel any direction other than along the diameter of the semicircle. The steel pipe also protects the user from direct contact with the x ray beam. The portion of the collimator nearest to the source needed to be thicker than that of the rest of the collimator. This is because the intensity of the x rays is much higher near the window of the source than by the sample. With this set up the radiation level just outside of the

collimator is at background. The extended length of the second section of the collimator decreases the uncertainty in theta. This will be looked into with more detail once the steel encasement is completed.

### 3.3 Mechanical Design

The design of the Houghton diffractometer follows that of a Bragg-Brentano  $\theta$ - $2\theta$  x ray diffractometer. The components necessary for this setup will be described in detail in this section.

#### 3.3.1 The Table

The entire apparatus is set on a standard 1.830 m x 1.219 m lab table. The mechanical system and the x ray source are both mounted to the top of the table. A diagram of a top down view can be seen in Figure 21. The x ray source is positioned in line with the diameter of the semicircle. The radius of the semicircle is 0.606 m. The  $\theta$  arm, which holds the sample, rotates from 0 to  $90^\circ$  by a LIN Engineering stepper motor. The  $2\theta$  arm, which holds the sensor, rotates to twice the angle of the  $\theta$  arm by another stepper motor. Since the incident and reflected angles of the x rays are symmetrical, the intensity of the reflected x rays can be measured using the  $\theta$ - $2\theta$  relationship of the mechanical arms. The underside of the table contains the rest of the apparatus: the HV acrylic box, computer, multimeters, and the cooling system.

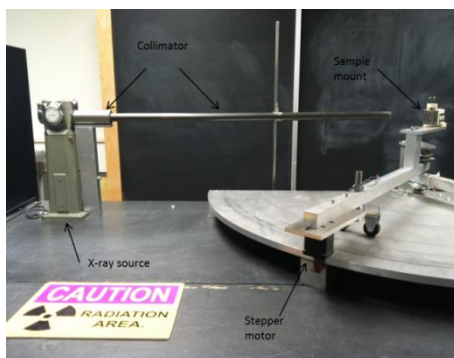


Figure 20: Picture including x ray source, collimator, and a portion of the mechanical system. The collimator both directs the x rays towards the sample mount and decreases the intensity of the x rays that travel through the walls of the collimator

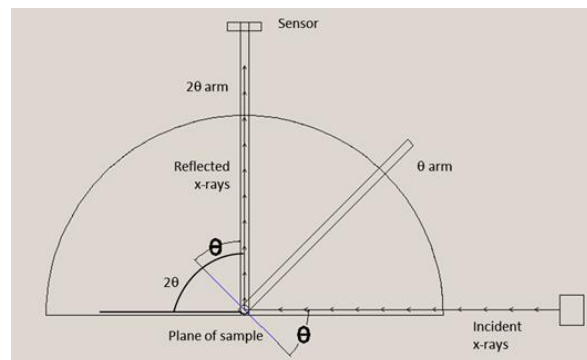


Figure 21: Basic diagram of a Bragg-Brentano  $\theta$ - $2\theta$  x ray diffractometer. The Houghton diffractometer follows this design. The  $\theta$  arm containing the sample rotates 0 to  $90^\circ$  while the  $2\theta$  arm containing the sensor rotates at twice the angle of the  $\theta$  arm.

### *3.3.2 Arms and Stepper Motors*

The arms were constructed from 25.40 mm x 25.40 mm aluminum rod. Both arms rotate around the central axis via the stepper motors, which can be seen in Figure 22. Both stepper motors have an axle that spins, rotating the arm around the semicircle. They are fitted with rubber tubing to ensure full contact and smooth motion around the outside of the semicircle. The stepper motors are run by a National Instruments (NI) Power Drive (MID-7604) which is controlled by a program written in LabVIEW. The program ensures a  $\theta$ - $2\theta$  relationship between the mechanical arms.

### *3.3.3 Sample Mount*

A picture of the sample mount can be seen in Figure 23. A 25.40 mm x 50.80 mm x 76.20 mm aluminum bar holds a 50.80 mm x 203.20 mm x 6.350 mm aluminum plate, containing a three dimensional micrometer, above the  $\theta$  arm. It is held above the  $\theta$  arm such that it is at the same elevation as the center of the x ray beam (0.2670 m above the tabletop). The micrometer positioned at the back of the mount will be used to center the sample over top of the central axis of the arms.

## **3.4 Safety Features**

Safety has been the main focus throughout the current phase of the construction of the x ray diffractometer. In order to complete the diffractometer it is important to ensure it will be safe for all of its users and those in the area.

### *3.4.1 HV Acrylic Box*

In order to protect against contact with HV components, the circuit that is used to run the x ray source is contained within an acrylic box. The box also prevents the HV components from shorting, which would disrupt x ray production. The box is located under the lab table just beneath the x ray source, seen in Figure 24. An interlock will be added such that, if the door is open, the HV supply won't be able to turn on.

### *3.4.2 Steel Encasement with Interlocks*

To ensure the safety of everyone involved with the diffractometer, a steel box surrounding the setup is necessary. The purpose of the box is to reduce the radiation level experienced by the participants to

background level (0.05mRem/hr.) While running the tests to determine the max intensity of the x ray source, the function of the collimator was tested. It was found that the 0.610 m section of the collimator, which is 3.1750 mm thick, reduced the intensity of the x rays to background. The measurement for this intensity was taken at the surface of the collimator. Due to this, it was decided that the steel encasement was to be 3.1750 mm thick. A graph of the performance of the x ray source can be seen in Chapter 4. A picture of the partially completed steel encasement can be seen in Figure 25. It is split up into 11 different panels. Each panel is attached to the table and adjacent panels via 3.1750 mm angle iron. The angle iron serves a double purpose. It fixes the panels to the table and each other, but also overlaps any partition between panels, assuring that the box has no openings. The side of the box near the source and flat portion of the semicircle will contain two doors, which will open downwards via long piano hinges. Magnets will be used at the top to fasten the two doors shut. These magnets will be utilized in the construction of an interlocking system. There are a few places within the steel box where the 3.1750 mm steel will not be enough to reduce the x rays to background. The first place is on the other side of the semicircle across from the collimator. Lead bricks will be used to reduce the intensity of the x rays before they go through the steel. The other point of concern is the side across from the doors. The reason this side is a concern is because when the x rays constructively interfere there will be an intense beam directed towards that wall. A sheet of lead will be placed along the back wall to protect against this. With the steel box in place, along with lead in the described position, the box will ensure the users are safe from any radiation hazards.

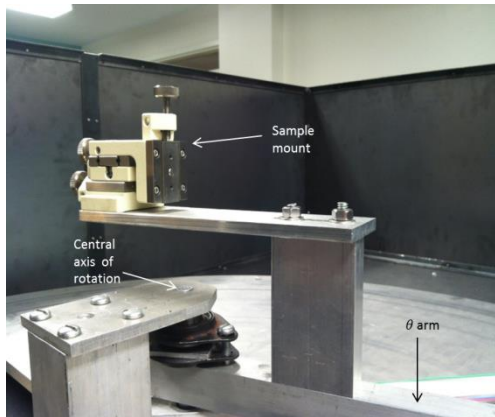


Figure 22: Stepper motor for the  $2\theta$  arm. The rubber tubing can be seen around the axle.

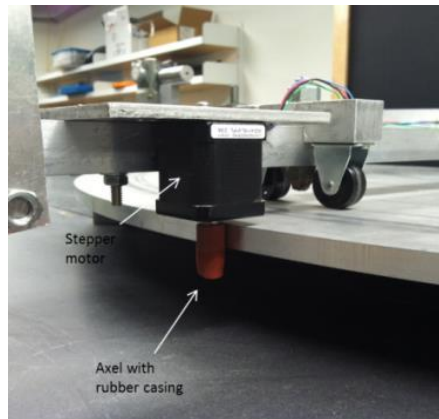


Figure 23: The three dimensional micrometer along with the aluminum plate and bar server as the sample mount for the diffractometer. The micrometer allows for accurate positioning of the sample above the central axis of the arms.

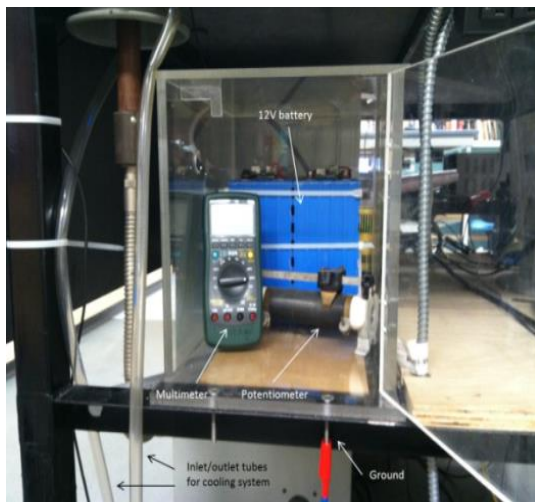


Figure 24: The HV acrylic box can be seen containing a multimeter, potentiometer, and battery, all of which are used in a circuit that powers the x ray source (wires omitted). This circuit can be seen in Fig. 18. The HV box is positioned below the source, which is mounted to the tabletop above it.

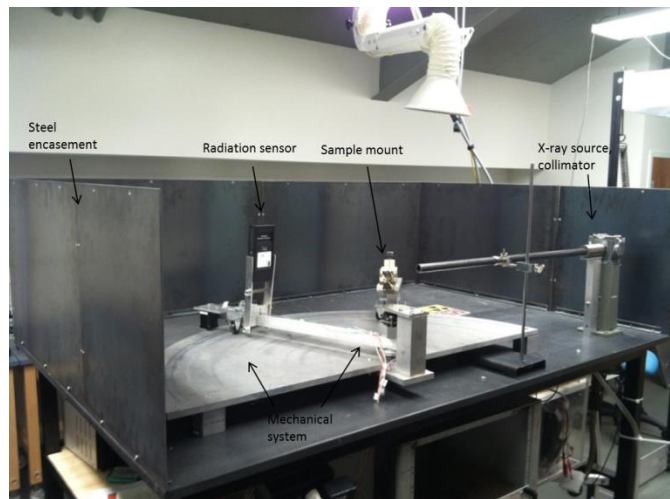


Figure 25: A picture of the partially completed steel encasement. The side walls can be seen, omitting the doors and the top.

RESULTS

**Intensity of X ray Source**

A series of tests were conducted to find the initial intensity of the x ray source. A set of precautionary measures was used for each test to ensure the safety of the participants. At the receiving end of the x ray beam lead bricks were placed to reduce the intensity of the beam to background level. Prior to collecting each data point, the emission current was slowly raised to its required value while the radiation intensity was measured at various points surrounding the lab table. A long steel arm with a clamp was used to hold the survey meter for each measurement.

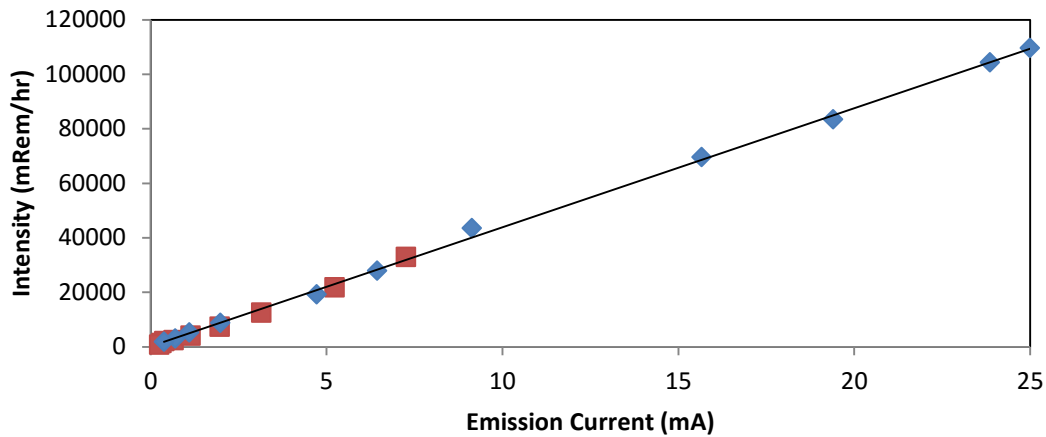


Figure 26: Graph of the intensity of the x ray source just outside of the window on the side of the source. The square data points were collected with a 25.40 mm aluminum block just outside the window of the source, between the source and the detector. A 50.80 mm aluminum block was used for the diamond data points. The 40 kV HV supply was used.

Figure 26 is a graph of the performance of the current x ray source while powered by the 40 kV power supply. A Ludlum Measurements Model 3 Survey Meter was used to measure the intensity of the x rays. A multimeter was used in series with the 40 kV supply and the filament to measure the emission current. Since the survey meter was only capable of reading intensities up to 200 Rem/hr, various blocks of aluminum were placed between the source and the survey meter to reduce the intensity. For

half of the data, a 25.40 mm (1 in.) aluminum block was set in place. For the rest of the data, a 50.80 mm (2 in.) block of aluminum was used. The survey meter was placed up against the aluminum block in line with the x ray beam. The following equation was used to relate the two data sets and determine the max intensity of the source if there was no aluminum block in place:

$$I = I_0 e^{-\mu_l z}, \quad (12)$$

where  $I$  is the intensity after the x rays pass through the aluminum,  $I_0$  is the initial intensity of the x rays at the window of the source,  $\mu_l$ , is the linear attenuation coefficient of aluminum, and  $z$  is the thickness of the material that the x rays pass through. A linear relationship should be expected between the intensity of the x rays and the emission current. Since an electron fired from the filament has a given probability of interacting with the target material and producing an x ray, the number of x rays is expected to be directly proportional to the number of electrons. Since the number of electrons is directly proportional to the emission current, then the intensity of the x rays is directly proportional to the emission current. Thus,

$$I = C * i_{em} = I_0 e^{-\mu_l z}, \quad (13)$$

where  $C$  is a constant. Letting  $I_1$  be the data set collected with the 25.40 mm aluminum block and  $I_2$  the data set collected with the 50.80 mm aluminum block,

$$I_1 = C_1 * i_{em} = I_0 e^{-\mu_l z_1} \quad (14)$$

and

$$I_2 = C_2 * i_{em} = I_0 e^{-\mu_l z_2}. \quad (15)$$

From a linear fit set to both data sets,

$$I_1 = 33.819i_{em} - 4.95 = I_0 e^{-\mu_l z_1} \quad (16)$$

and

$$I_2 = .2514i_{em} + .0115 = I_0 e^{-\mu_l z_2}. \quad (17)$$

First solve for  $\mu_l$  by letting  $i_{em} = 10\text{mA}$ ,  $z_1 = 25.40\text{ mm}$ ,  $z_2 = 50.40\text{ mm}$ , then dividing Eq. 17 by Eq. 16 resulting in

$$\mu_l = 4.88\text{ in}^{-1} = 1.92\text{ cm}^{-1}. \quad (18)$$

According to the National Institute of Standards and Technology (NIST), the attenuation coefficient per density,  $\frac{\mu}{\rho}$ , for aluminum is

$$0.5685 \frac{\text{cm}^2}{\text{g}} \leq \frac{\mu}{\rho} \leq 1.128 \frac{\text{cm}^2}{\text{g}} \quad (19)$$

for electron energies between 30 keV and 40 keV [30]. The value calculated value of  $\mu_l$  in this experiment divided by  $\rho_{Al} = 2.70 \frac{\text{g}}{\text{cm}^3}$  is

$$\frac{\mu}{\rho} = 0.711 \frac{\text{cm}^2}{\text{g}}. \quad (20)$$

Using the calculated value of  $\mu_l$ , the intensity of the beam just before passing through the aluminum blocks was determined. This intensity can be seen in Figure 26. At a max input of 25 mA, the source has an output intensity of 110 Rem/hr. Once the steel box is constructed, measurements will be taken to determine the number of x rays produced by the source.

## Chapter 5

### CONCLUSIONS

#### 5.1 Current Status

Overall, the x ray diffractometer is nearing a state where it can be used to analyze a silver thin film that was produced in the deposition chamber.

##### 5.1.1 X ray Source

The x ray source is currently operational. As seen in Chapter 4, the maximum intensity of the source was determined. The next step is to see if the source produces an adequate number of x rays, as seen by the radiation sensor on the  $2\theta$  arm. This test will be run once the steel encasement is completed. If an inadequate number of x rays are read by the sensor, further modifications to the apparatus must be made.

##### 5.1.2 Steel Encasement

Currently, the walls and the doors of the steel encasement are mounted to the lab table. Once the top is completed, construction of the interlocking system will begin. Also, lead bricks will be placed in line with the x ray beam on the opposite side of the encasement compared to the source. A sheet of lead will be placed along the back wall of the encasement as well. This will ensure that, while the source is on, the radiation level experienced by the user is at 0.05 mRem/hr or less.

##### 5.1.3 LabVIEW Program

The program used to run the stepper motors and the radiation sensor is almost complete. A few changes need to be made to make it more efficient and user friendly. Currently, the program is able to read in data from the radiation detector and move the stepper motors. As for data collection, there has yet to be an efficient program written to save and export a file containing the data. Also, if a run is stopped before the initial set time, the data is not saved. As for the motors, the program that will maintain the  $\theta$ - $2\theta$  relationship between the arms has been written. The program rotates the  $2\theta$  arm

twice as fast as the  $\theta$  arm to keep the desired relationship. While the program is believed to have been written without error, the  $\theta$ - $2\theta$  relationship is unable to be maintained. The reason behind this will be discussed in section 5.1.4

#### *5.1.4 Stepper Motors*

As stated above in Section 5.1.3, the stepper motors are unable to maintain the  $\theta$ - $2\theta$  relationship they are supposed to. This is believed to be caused by the aluminum semicircle. The semicircle was intended to be 0.6064 m radius, but the actual radius is 1.0 to 3.0 mm larger at certain points. This results in the axle of the motor fitting tighter to the outside of the semicircle. This larger frictional force causes the axle's rotational speed to decrease. The current plan is to both sand and file the section of the semicircle that has a larger radius until the issue has resided. If this plan does not work, further planning of the motor set up will be required.

## **5.2 Future Plans**

A few plans are in place to improve the performance and safety of the Houghton diffractometer.

### *5.2.1 Interlocking System*

As mentioned briefly in Section 3.5.2, an interlocking system will be constructed for the safety of the users. It will be built once the steel encasement is completed. The interlocking system will utilize a pin on the back of the HV supply that needs to be grounded. This pin will be connected in series with a wire that connects the doors of the steel encasement, collimator, and the latch on the door of the acrylic box. When any of these objects are open or removed, the connection to ground will be broken and the HV supply will shut off.

### *5.2.2 Cooling System with Flowmeter*

A water chiller will be added to the cooling system, which will assure cold water is being supplied to the target and will also allow for the use of distilled water. A flowmeter will be connected to the drain hose. If the flow of water through the meter is not sufficient for the cooling of the target, the HV supply will shut off, preventing the target from being damaged.

### 5.2.3 *Web Camera*

A web camera will be mounted inside the steel box so the apparatus can be monitored while it is running. LEDs will be mounted alongside the camera to increase visibility. The camera will help to identify the sources of any problems that arise.

## References

- [1] I. Newton, *Opticks: Or A Treatise of the Reflections, Refractions, Inflections and Colours of Light*, 4th Edition, (1730), pp.41.
- [2] Example of Newton's rings ([https://en.wikipedia.org/wiki/Newton%27s\\_rings#/media/File:20cm\\_Air\\_1.jpg](https://en.wikipedia.org/wiki/Newton%27s_rings#/media/File:20cm_Air_1.jpg)).
- [3] T. Young, Philos. Trans. R. Soc. London **92**, 34 (1802).
- [4] T. Young, *A Course of Lectures on Natural Philosophy and the Mechanical Arts*, Vol. 2 (William Savage, London, 1807), pp. 463-464.
- [5] N. Robotti, Rend. Fis. Acc. Lincei **24**, S7-S8 (2013).
- [6] Crookes Tube diagram (<http://reich-chemistry.wikispaces.com/422-004+K.+Dickson+%26amp+%3B+S.+Lindo+Big+Timeline+Project>).
- [7] A. Stanton, *Nature (London)* **53**, 274 (1896).
- [8] M. Laue, *Concerning the detection of X-ray interferences*, Nobel Lecture (Unpublished).
- [9] W. H. Bragg and W. L. Bragg, *X-rays and Crystal Structure* (G. Bell and Sons, LTD., London, 1915), pp. 8-25.
- [10] P. P. Ewald, *Fifty years of X-ray diffraction* (A. Oosthoek's Uitgeversmij, Utrecht, 1962), pp.120, 125.
- [11] H. P. Rooksby, J. Sci. Intsrum. **18**, 84-90 (1941).
- [12] W. A. Wood, Trans. Faraday Soc. **31**, 1248-1263 (1935).
- [13] G. V. Marr, *Handbook on Synchrotron Radiation: Vacuum Ultraviolet and Soft X-ray Processes*, Vol. 2 (North Holland Pub. Co., New York, 1987), pp. 3.
- [14] M. Caffrey and D. H. Bilderback, Nucl. Instrum. Methods in Phys. Res. 208 (1), 495 (1983).
- [15] Coolidge, William D, Patent No. 1,502,907 (July 29, 1924).
- [16] G. M. Alonzo-Medina *et al*, 2013 IOP Conf. Proc.: Materials Science and Engineering **45**, 1 (2013).
- [17] N. K. Ponon *et al*, Thin Solid Films **578**, 31-37 (2015).
- [18] S. P. Baker *et al*, Acta Materialia **61**, 7121 (2013).
- [19] J. Mertzlufft, B.S. Thesis (Houghton College, New York, 2013, unpublished).
- [20] E. Ocock, B.S. Thesis (Houghton College, New York, 2014, unpublished).
- [21] T. Reynolds, B.S. Thesis (Houghton College, New York, 2013, unpublished).
- [22] J. Yuly, B.S. Thesis (Houghton College, New York, 2016, unpublished).
- [23] S. Daigler B.S. Thesis (Houghton College, New York, 2015, unpublished).
- [24] Characteristic X rays, [http://www.amptek.com/pdf/characteristic\\_xrays.pdf](http://www.amptek.com/pdf/characteristic_xrays.pdf).
- [25] Characteristic/Bremsstrahlung Diagram, [http://www2.rgu.ac.uk/life\\_semweb/xray.html](http://www2.rgu.ac.uk/life_semweb/xray.html).
- [26] B. Van Zeghbroeck, *Principles of Semiconductor Devices*, (Unpublished, 2011).
- [27] C. Hammond, *The Basics of Crystallography and Diffraction*, 3<sup>rd</sup> Ed. (Oxford University Press, NY, 2009), p. 6.

- [28] ccp Structure, <http://www.chem.fsu.edu/chemlab/chm1046course/solids.html>.
- [29] Norelco X ray Analytical Instrumentation Manual.
- [30] Hubbell, J.H. and Seltzer, S.M. (2004), Tables of X-Ray Mass Attenuation Coefficients and Mass Energy-Absorption Coefficients (version 1.4). [Online] Available: <http://physics.nist.gov/xaamdi> [2016, Dec 4].